

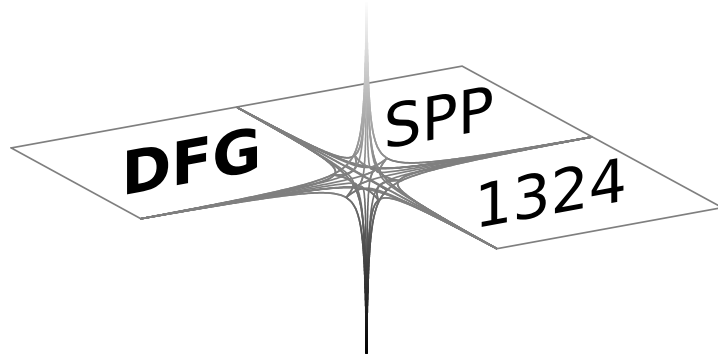
# DFG-Schwerpunktprogramm 1324

„Extraktion quantifizierbarer Information aus komplexen Systemen“

## An iterative reconstruction scheme for photoacoustic imaging

Y. Dong, T. Görner, S. Kunis

Preprint 114



Edited by

AG Numerik/Optimierung  
Fachbereich 12 - Mathematik und Informatik  
Philipps-Universität Marburg  
Hans-Meerwein-Str.  
35032 Marburg

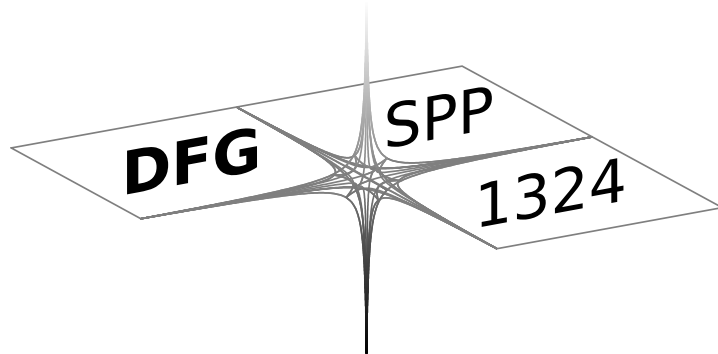
# DFG-Schwerpunktprogramm 1324

„Extraktion quantifizierbarer Information aus komplexen Systemen“

## An iterative reconstruction scheme for photoacoustic imaging

Y. Dong, T. Görner, S. Kunis

Preprint 114



The consecutive numbering of the publications is determined by their chronological order.

The aim of this preprint series is to make new research rapidly available for scientific discussion. Therefore, the responsibility for the contents is solely due to the authors. The publications will be distributed by the authors.

# An iterative reconstruction scheme for photoacoustic imaging

Yiqiu Dong<sup>†</sup>      Torsten Görner<sup>‡</sup>      Stefan Kunis<sup>§</sup>

Recovery of image data from photoacoustic measurements asks for the inversion of the spherical mean value operator. In contrast to direct inversion methods for specific geometries, we consider a semismooth Newton scheme to solve a total variation regularized least squares problem. During the iteration, each matrix vector multiplication is realized in an efficient way using a recently proposed spectral discretization of the spherical mean value operator. All theoretical results are illustrated by numerical experiments.

*Key words and phrases* : spherical mean operator, fast Fourier transform, total variation regularization, photoacoustic imaging.

*2010 AMS Mathematics Subject Classification* : 65T50, 44A12, 92C55.

## 1 Introduction

Analogously to the Radon transform for computerized tomography, the spherical mean value operator is the crucial ingredient in photoacoustic imaging [31, 21, 4]. Recovery of image data from photoacoustic measurements hence asks for the inversion of this operator and this problem has been studied recently in [9, 3, 1, 21, 28] and references therein. For specific geometries, direct reconstruction algorithms are discussed in [14, 25, 24, 13, 2, 8, 23, 11] and in contrast to point-like detectors in the above model, variants for integrating detectors have been studied in [12, 5, 26, 34, 15, 33].

In this paper we consider the case of center points located at an arbitrary submanifold where direct reconstruction formulae are unknown. In order to reconstruct images from photoacoustic measurements stably, regularization techniques are utilized. In this direction and with the aim of preserving significant edges in images, we consider the total variation regularization, which was proposed in [29] and is well known in image restoration. Then, we set up an iterative method to solve the total variation regularized least squares problem based on the Fenchel-duality and inexact semismooth Newton techniques following the approach in

---

<sup>†</sup>Helmholtz Zentrum München, Institute for Biomathematics and Biometry, yiqiu.dong@helmholtz-muenchen.de

<sup>‡</sup>University Osnabrück, Institute of Mathematics, torsten.goerner@uos.de

<sup>§</sup>University Osnabrück, Institute of Mathematics, and Helmholtz Zentrum München, Institute for Biomathematics and Biometry, stefan.kunis@math.uos.de

[17]. In each iteration, we apply the recently proposed algorithm [10] for the fast and accurate computation of spherical means.

The structure of our paper is as follows. Section 2 reviews the Cauchy problem for the wave equation and its relation to the spherical mean value operator. After discretization of this operator via trigonometric polynomials, we discuss the algorithmic properties of this discrete spherical mean value operator. The following section sets up the total variation regularized least squares problem ( $P_0$ ) and studies a tight relaxation for which the semismooth Newton method [27, 16] is applied. Several numerical experiments are reported in Section 4 and we conclude our findings in the last section.

## 2 Photoacoustic imaging, spherical means, and discretization

In many topics of photoacoustic imaging we have to deal with the Cauchy problem for the wave equation

$$\begin{aligned} \partial_t^2 p(\mathbf{x}, t) - \nu_s^2(\mathbf{x}) \Delta p(\mathbf{x}, t) &= 0 \quad \text{for } (\mathbf{x}, t) \in \mathbb{R}^d \times (0, \infty), \\ p(\mathbf{x}, 0) &= f(\mathbf{x}) \quad \text{for } \mathbf{x} \in \mathbb{R}^d, \\ \partial_t p(\mathbf{x}, 0) &= 0 \quad \text{for } \mathbf{x} \in \mathbb{R}^d, \end{aligned} \tag{2.1}$$

where  $d \in \mathbb{N}$ ,  $d \geq 2$ , is the spatial dimension,  $p$  is the pressure and  $\nu_s$  is the speed of sound within the medium. In general, the speed of sound depends on the spatial variable  $\mathbf{x}$ , but many setups allow to assume homogeneity and consequently, after rescaling, we suppose  $\nu_s = 1$ . It is well known [7, §13, eq. 13-15] that for a sufficiently smooth function  $f : \mathbb{R}^d \rightarrow \mathbb{R}$  the solution of (2.1) can be given as

$$p(\mathbf{x}, t) = \begin{cases} \frac{1}{\Gamma(\frac{d}{2})2^{d-1}} (t^{-1} \frac{\partial}{\partial t})^{\frac{d}{2}} \int_0^t \frac{r}{\sqrt{t^2-r^2}} (r^{-1} \frac{\partial}{\partial r})^{\frac{d-2}{2}} r^{d-2} (\mathcal{M}f)(\mathbf{x}, r) dr & \text{for even } d, \\ \frac{\sqrt{\pi}}{\Gamma(\frac{d}{2})2^{\frac{d-1}{2}}} \frac{\partial}{\partial t} (t^{-1} \frac{\partial}{\partial t})^{\frac{d-3}{2}} (t^{d-2} (\mathcal{M}f)(\mathbf{x}, t)) & \text{for odd } d, \end{cases}$$

where the spherical mean value operator  $\mathcal{M}$  is defined by

$$\mathcal{M}f(\mathbf{x}, r) := \frac{1}{\omega_{d-1}} \int_{\mathbb{S}^{d-1}} f(\mathbf{x} + r\boldsymbol{\xi}) d\sigma(\boldsymbol{\xi}), \quad (\mathbf{x}, r) \in \mathbb{R}^d \times \mathbb{R}.$$

Here,  $\mathbb{S}^d := \{\mathbf{x} \in \mathbb{R}^d : |\mathbf{x}|_2^2 := \sum_{j=1}^d x_j^2 = 1\}$  denotes the  $d-1$  dimensional sphere,  $\sigma$  denotes the surface measure on  $\mathbb{S}^{d-1}$  and  $\omega_{d-1} := \sigma(\mathbb{S}^{d-1})$ . The goal is to recover  $f$ , if  $p(\mathbf{x}, t)$ ,  $(\mathbf{x}, t) \in \Omega \times \mathbb{R}$ , is known, where  $\Omega \subset \mathbb{R}^d$  is some submanifold surrounding the region of interest. In particular for spatial dimension  $d = 3$ , we have to find  $f(\mathbf{x})$ ,  $\mathbf{x} \in \mathbb{R}^3$ , from the data

$$p(\mathbf{x}, t) = \frac{\partial}{\partial t} (t (\mathcal{M}f)(\mathbf{x}, t)), \quad \mathbf{x} \in \Omega \subset \mathbb{R}^3, \quad t \in \mathbb{R}.$$

In this paper, we limit our considerations to recovering a function from its spherical means with iterative methods. For this purpose, the efficient and accurate computation of spherical means from given function values on some grid is essential. We follow our recent approach in [10] and restrict to functions supported on  $[-\frac{1}{2}, \frac{1}{2}]^d =: \mathbb{T}^d$ , which are approximated by trigonometric polynomials. The spherical mean value operator is bounded from  $L^p(\mathbb{T}^d)$  to

$L^p(\mathbb{T}^d \times [0, 1], d\mathbf{y}r^{d-1} dr)$ , and allows for a decomposition in eigenfunctions  $e_{\mathbf{k}} : \mathbb{T}^d \rightarrow \mathbb{C}$ ,  $e_{\mathbf{k}}(\mathbf{x}) = e^{2\pi i \mathbf{k} \mathbf{x}}$ ,  $\mathbf{k} \in \mathbb{Z}^d$ ,

$$\mathcal{M}e_{\mathbf{k}}(\mathbf{y}, r) = e_{\mathbf{k}}(\mathbf{y}) \frac{\Gamma\left(\frac{d}{2}\right) J_{\frac{d-2}{2}}(2\pi|\mathbf{k}|_2 r)}{(\pi|\mathbf{k}|_2 r)^{\frac{d-2}{2}}},$$

where  $J$  denotes the Bessel function of first kind. For some discretization parameter  $n \in \mathbb{N}$ , the function  $f : \mathbb{T}^d \rightarrow \mathbb{R}$  is typically given by discrete values  $f(\mathbf{x})$  on a regular grid  $\mathbf{x} \in X \subset \mathbb{T}^d$ ,

$$X := \left\{ \left( \frac{2j_1+1-n}{2n}, \dots, \frac{2j_d+1-n}{2n} \right)^\top, \mathbf{j} \in [0, n)^d \cap \mathbb{Z}^d \right\},$$

and the spherical means  $\mathcal{M}f(\mathbf{y}, r)$  have to be computed for scattered center points  $\mathbf{y} \in Y \subset \mathbb{T}^d$  and radii  $r \in R \subset [0, 1]$ . To this end, we compute discrete Fourier coefficients

$$\hat{f}_{\mathbf{k}} := \sum_{\mathbf{x} \in X} f(\mathbf{x}) e^{-2\pi i \mathbf{k} \mathbf{x}}, \quad \mathbf{k} \in J_n := \left[ -\frac{n}{2}, \frac{n}{2} \right)^d \cap \mathbb{Z}^d,$$

by one ordinary fast Fourier transform (FFT) in a first step. Subsequently, we compute for each radius  $r \in R$  auxiliary coefficients

$$\tilde{h}_{\mathbf{k}, r} := \hat{f}_{\mathbf{k}} \frac{\Gamma\left(\frac{d}{2}\right) J_{\frac{d-2}{2}}(2\pi|\mathbf{k}|_2 r)}{(\pi|\mathbf{k}|_2 r)^{\frac{d-2}{2}}}, \quad \mathbf{k} \in J_n,$$

and evaluate

$$\mathcal{M}f(\mathbf{y}, r) \approx g(\mathbf{y}, r) := \sum_{\mathbf{k} \in J_n} \tilde{h}_{\mathbf{k}, r} e^{2\pi i \mathbf{k} \mathbf{y}}, \quad \mathbf{y} \in Y,$$

by nonequispaced FFTs. In matrix vector notation, this sums up to

$$\mathbf{g} = \mathbf{M} \mathbf{f},$$

with a discrete spherical mean value operator  $\mathbf{M} : \mathbb{R}^N \rightarrow \mathbb{C}^M$ ,  $N = n^d$ ,  $M = M_1 M_2$ ,  $M_1 = |Y|$ ,  $M_2 = |R|$ ,

$$\mathbf{M} = \begin{pmatrix} \mathbf{A} \mathbf{D}_1 \mathbf{F} \\ \mathbf{A} \mathbf{D}_2 \mathbf{F} \\ \vdots \\ \mathbf{A} \mathbf{D}_{M_2} \mathbf{F} \end{pmatrix},$$

with the following nonequispaced Fourier matrix  $\mathbf{A} \in \mathbb{C}^{M_1 \times N}$ , diagonal matrices  $\mathbf{D}_j \in \mathbb{R}^{N \times N}$ ,  $j = 1, \dots, M_2$ , and a Fourier matrix  $\mathbf{F} \in \mathbb{C}^{N \times N}$ ,

$$\begin{aligned} (\mathbf{A})_{\mathbf{y}, \mathbf{k}} &= e^{2\pi i \mathbf{k} \mathbf{y}}, & \mathbf{y} \in Y, \mathbf{k} \in J_n, \\ (\mathbf{D}_j)_{\mathbf{k}, \mathbf{k}} &= \frac{\Gamma\left(\frac{d}{2}\right) J_{\frac{d-2}{2}}(2\pi\|\mathbf{k}\|_2 r_j)}{(\pi\|\mathbf{k}\|_2 r_j)^{\frac{d-2}{2}}}, & \mathbf{k} \in J_n, \\ (\mathbf{F})_{\mathbf{k}, \mathbf{x}} &= e^{-2\pi i \mathbf{k} \mathbf{x}}, & \mathbf{k} \in J_n, \mathbf{x} \in X. \end{aligned}$$

An immediate consequence is given by

**Lemma 2.1.** *With the above definitions, we have*

$$\mathbf{M}^* \mathbf{M} = \mathbf{F}^* \left( \sum_{j=1}^{M_2} \mathbf{D}_j \mathbf{T} \mathbf{D}_j \right) \mathbf{F}$$

with the hermitian multilevel Toeplitz matrix  $\mathbf{T} \in \mathbb{C}^{N \times N}$ ,

$$(\mathbf{T})_{\mathbf{k}, \mathbf{l}} = \sum_{\mathbf{y} \in Y} e^{2\pi i(\mathbf{k}-\mathbf{l})\mathbf{y}}.$$

*Proof.* We rewrite the above definition as

$$\mathbf{M} = \begin{pmatrix} \mathbf{A} & & \\ & \ddots & \\ & & \mathbf{A} \end{pmatrix} \begin{pmatrix} \mathbf{D}_1 \\ \vdots \\ \mathbf{D}_{M_2} \end{pmatrix} \mathbf{F}$$

and use

$$(\mathbf{A}^* \mathbf{A})_{\mathbf{k}, \mathbf{l}} = \sum_{\mathbf{y} \in Y} e^{2\pi i(\mathbf{k}-\mathbf{l})\mathbf{y}}$$

■

As detailed in [10], the above approach leads to an algorithm of complexity  $\mathcal{O}(M_2(N \log N + M_1))$  in general using the nonequispaced FFT [20]. For the two-dimensional case, i.e.  $n \times n$  images,  $M_1 = M_2 = \mathcal{O}(n)$  detectors and radii, this leads to a semi-fast method of complexity  $\mathcal{O}(n^3 \log n)$ . In case  $d = 3$ , i.e.  $n \times n \times n$  volumes,  $M_1 = \mathcal{O}(n^2)$  detectors and  $M_2 = \mathcal{O}(n)$  radii, this can be improved by the recently proposed butterfly sparse FFT [32, 22] and leads to an algorithm of complexity  $\mathcal{O}(n^3 \log n)$ .

We note in passing that the considered trigonometric interpolation is complex valued also for real valued functions, but can easily be made real valued by extending the discrete Fourier coefficients  $\hat{f}_{\mathbf{k}}$  to  $[-\frac{n}{2}, \frac{n}{2}]^d \cap \mathbb{Z}^d \supset J_n$  appropriately. Subsequently, we consider this real valued discrete spherical mean value operator and for ease of notation the two-dimensional case.

### 3 TV-Based Iterative Method

We now turn to the reconstruction problem

$$\mathbf{M} \mathbf{f} = \mathbf{g}, \tag{3.1}$$

where  $\mathbf{g} \in \mathbb{R}^M$  is the vector of discrete spherical mean values,  $\mathbf{f} \in \mathbb{R}^N$  is a real valued image obtained from a two-dimensional  $n$ -by- $n$  pixel-array on a regular grid by concatenation in the usual columnwise fashion with  $N = n^2$ , and  $\mathbf{M} \in \mathbb{R}^{M \times N}$  is the discrete spherical mean value operator. The problem of reconstructing the image  $\mathbf{f}$  from the measurements  $\mathbf{g}$  is known to be ill-posed. Hence, regularization techniques based on prior information on  $\mathbf{f}$  are utilized to get stable reconstruction processes. In this direction, total variation (TV) regularization [29] had great success, which is defined by

$$\|\mathbf{v}\|_{\text{TV}} := \sum_{k=1}^N \|\nabla \mathbf{v}\|_k = \sum_{k=1}^N \sqrt{|\nabla_x \mathbf{v}|_k^2 + |\nabla_y \mathbf{v}|_k^2}.$$

Here, we use the abbreviation  $[\mathbf{p}]_k = (p_k, p_{N+k})^\top$ ,  $\mathbf{p} \in \mathbb{R}^{2N}$ ,  $k = 1, \dots, N$ , and define the discrete gradient operator  $\nabla \in \mathbb{R}^{2N \times N}$  by  $[\nabla \mathbf{v}]_k := ((\nabla_x \mathbf{v})_k, (\nabla_y \mathbf{v})_k)^\top$  with the forward differences

$$(\nabla_x \mathbf{v})_k = \begin{cases} \mathbf{v}_{s+1,t} - \mathbf{v}_{s,t}, & \text{if } s < n, \\ 0, & \text{if } s = n, \end{cases} \quad (\nabla_y \mathbf{v})_k = \begin{cases} \mathbf{v}_{s,t+1} - \mathbf{v}_{s,t}, & \text{if } t < n, \\ 0, & \text{if } t = n, \end{cases}$$

and  $k = sn + t$  with  $(s, t) \in \{1, 2, \dots, n\} \times \{1, 2, \dots, n\}$  as an index in the regular pixel-array. Combining the TV regularization with an  $l^2$ -data-fitting term, we reconstruct the image  $\mathbf{f}$  by solving the minimization problem

$$\min_{\mathbf{f} \in \mathbb{R}^N} \mathcal{J}(\mathbf{f}), \quad \mathcal{J}(\mathbf{f}) := \frac{1}{2} \|\mathbf{M}\mathbf{f} - \mathbf{g}\|_2^2 + \alpha \|\mathbf{f}\|_{\text{TV}}, \quad (P_0)$$

where  $\alpha > 0$  is the regularization parameter to control the trade-off between a good fitness to  $\mathbf{g}$  and the smoothness from the TV term.

The TV term is nondifferentiable and this is responsible for preserving edges in images but also poses an algorithmic challenge. In order to overcome the difficulty, referring to [17] we utilize Fenchel duality and introduce associated inexact semismooth Newton techniques. Applying the Fenchel-Legendre duality calculus, we derive the Fenchel-dual of  $(P_0)$

$$\begin{aligned} \sup_{\mathbf{p} \in \mathbb{R}^{2N}} & -\frac{1}{2} \|\mathbf{M}^* \mathbf{g} - \text{div} \mathbf{p}\|_{\mathbf{M}}^2 + \frac{1}{2} \|\mathbf{g}\|_2^2, \\ \text{s.t.} & \quad \|\mathbf{p}\|_2 \leq \alpha, \quad \text{for all } k = 1, \dots, N, \end{aligned} \quad (P_0^*)$$

where  $\|\mathbf{v}\|_{\mathbf{M}}^2 := \langle (\mathbf{M}^* \mathbf{M})^{-1} \mathbf{v}, \mathbf{v} \rangle = \sum_{k=1}^N \mathbf{v}_k \cdot ((\mathbf{M}^* \mathbf{M})^{-1} \mathbf{v})_k$ , and the divergence operator is given by  $\text{div} = -\nabla^\top$ . Due to the nontrivial kernel of the divergence operator, the solution of  $(P_0^*)$  is not unique. To overcome the non-uniqueness of the solution of  $(P_0^*)$ , we propose a dual regularization

$$\begin{aligned} \sup_{\mathbf{p} \in \mathbb{R}^{2N}} & -\frac{1}{2} \|\mathbf{M}^* \mathbf{g} - \text{div} \mathbf{p}\|_{\mathbf{M}}^2 + \frac{1}{2} \|\mathbf{g}\|_2^2 - \frac{\gamma}{2\alpha} \sum_{k=1}^N \|\mathbf{p}\|_k^2, \\ \text{s.t.} & \quad \|\mathbf{p}\|_k \leq \alpha, \quad \text{for all } k = 1, \dots, N, \end{aligned} \quad (P^*)$$

where  $\gamma > 0$  is the dual regularization parameter. In order to understand the effect of the dual regularization on the original minimization problem, we apply the Fenchel-Legendre calculus once more and find that the dual of  $(P^*)$  is given by

$$\min_{\mathbf{f} \in \mathbb{R}^N} \frac{1}{2} \|\mathbf{M}\mathbf{f} - \mathbf{g}\|_2^2 + \sum_{k=1}^N (\Phi_\gamma(\nabla \mathbf{f}))_k, \quad (P)$$

where

$$(\Phi_\gamma(\nabla \mathbf{f}))_k := \begin{cases} \frac{\alpha}{2\gamma} \|[\nabla \mathbf{f}]_k\|_2^2, & \text{if } \|[\nabla \mathbf{f}]_k\|_2 < \gamma, \\ \alpha (\|[\nabla \mathbf{f}]_k\|_2 - \frac{\gamma}{2}), & \text{if } \|[\nabla \mathbf{f}]_k\|_2 \geq \gamma. \end{cases}$$

Here,  $\Phi_\gamma$  is a Huber function [19], which smooths locally the TV term in order to obtain the differentiability of  $(P)$  and the uniqueness of the dual solution  $\mathbf{p}$ .

Based on the first order optimality condition, the solution  $(\bar{\mathbf{f}}, \bar{\mathbf{p}})$  satisfies

$$\mathbf{M}^* \mathbf{M} \bar{\mathbf{f}} + \text{div} \bar{\mathbf{p}} = \mathbf{M}^* \mathbf{g}, \quad (3.2)$$

$$\max\{\gamma, |[\nabla \bar{\mathbf{f}}]_k|_2\} [\bar{\mathbf{p}}]_k = -\alpha [\nabla \bar{\mathbf{f}}]_k, \quad \text{for } k = 1, \dots, N.$$

Due to the presence of the max-operator, the system is not smooth but semismooth. We are able to solve it by the semismooth Newton technique, see [27, 16]. The semismooth Newton step is given by

$$\mathbf{f}^{l+1} = \mathbf{f}^l + \delta, \quad \mathbf{H}^l \delta = \mathbf{w}^l \quad (3.3)$$

with

$$\begin{aligned} \mathbf{H}^l &= \mathbf{M}^* \mathbf{M} + \nabla^\top \mathbf{D}(\mathbf{m}_{\gamma^l})^{-1} \left[ \alpha \mathbf{I}_N - \chi_{\mathcal{A}^l} \mathbf{D}(\mathbf{p}^l) \mathbf{N}(\nabla \mathbf{f}^l) \right] \nabla, \\ \mathbf{w}^l &= -\mathbf{M}^*(\mathbf{M} \mathbf{f}^l - \mathbf{g}) - \alpha \nabla^\top \mathbf{D}(\mathbf{m}_{\gamma^l})^{-1} \nabla \mathbf{f}^l. \end{aligned}$$

Here,  $\mathbf{I}_N \in \mathbb{R}^{N \times N}$  is the identity matrix,  $\mathbf{D}(\mathbf{m}_{\gamma^l}) \in \mathbb{R}^{2N \times 2N}$  is a diagonal matrix with the vector  $\mathbf{m}_{\gamma^l} \in \mathbb{R}^{2N}$ ,  $(\mathbf{m}_{\gamma^l})_k = (\mathbf{m}_{\gamma^l})_{N+k} = \max\{\gamma, |[\nabla \mathbf{f}^l]_k|_2\}$ , as the main diagonal. Moreover, we define the set  $\mathcal{A}^l = \{k : |[\nabla \mathbf{f}^l]_k|_2 > \gamma\}$  and the thresholding operator as diagonal matrix  $\chi_{\mathcal{A}} \in \mathbb{R}^{2N \times 2N}$ ,

$$(\chi_{\mathcal{A}})_{k,k} = (\chi_{\mathcal{A}})_{N+k,N+k} = \begin{cases} 1, & \text{if } k \in \mathcal{A}, \\ 0, & \text{if } k \in \mathcal{A}^c. \end{cases}$$

In addition, with  $\mathbf{v} = (\mathbf{v}_1^\top, \mathbf{v}_2^\top)^\top \in \mathbb{R}^{2N}$ , we set

$$\mathbf{N}(\mathbf{v}) = \begin{bmatrix} \mathbf{D}(\mathbf{v}_1) & \mathbf{D}(\mathbf{v}_2) \\ \mathbf{D}(\mathbf{v}_1) & \mathbf{D}(\mathbf{v}_2) \end{bmatrix} \in \mathbb{R}^{2N \times 2N}.$$

In general, the matrix  $\mathbf{H}^l$  is not symmetric, but at a solution it is symmetric positive semi-definite. In order to avoid problems due to these potential deficiencies during the iterations, we utilize the modifications as introduced in [17], whenever these are necessary. In addition, since there is no guarantee that  $\mathbf{H}^l$  is positive definite, a solution  $\delta$  in (3.3) may not exist or may not be unique in case of existence. As a remedy, we add a small multiple of the identity matrix to the system matrix and then solve it by biconjugate gradient stabilized (BICGSTAB) algorithm [30]. Similar as in [17] the whole algorithm can be shown to converge at a superlinear rate provided that  $\mathbf{f}^0$  is sufficiently close to the solution.

## 4 Numerical experiments

In this section, we provide numerical results to study the behavior of our method with respect to its image reconstruction capability and its computational efficiency. In our numerics, when solving the minimization problem (3.2), we set  $\gamma = 10^{-3}$ , and we stop the Newton iteration as soon as the initial residual is reduced by a factor of  $10^{-4}$ . In each Newton step, the BICGSTAB iteration is stopped as soon as the relative norm of the residual of the primal-dual system (3.2) at  $(\mathbf{f}^l, \mathbf{p}^l)$  drops below

$$\begin{aligned} \text{tol}^{l+1} &:= 10^{-3} \cdot \min \left\{ \left( \frac{\|\mathbf{r}^l\|_2}{\|\mathbf{r}^0\|_2} \right)^{\frac{3}{2}}, \frac{\|\mathbf{r}^l\|_2}{\|\mathbf{r}^0\|_2} \right\}, \\ \mathbf{r}^l &:= \begin{pmatrix} \mathbf{M}^* \mathbf{M} \mathbf{f}^l + \text{div} \mathbf{p}^l - \mathbf{M}^* \mathbf{g} \\ (\max\{\gamma, |[\nabla \mathbf{f}^l]_k|_2\} [\mathbf{p}^l]_k + \alpha [\nabla \mathbf{f}^l]_k)_{k=1, \dots, N} \end{pmatrix}. \end{aligned}$$

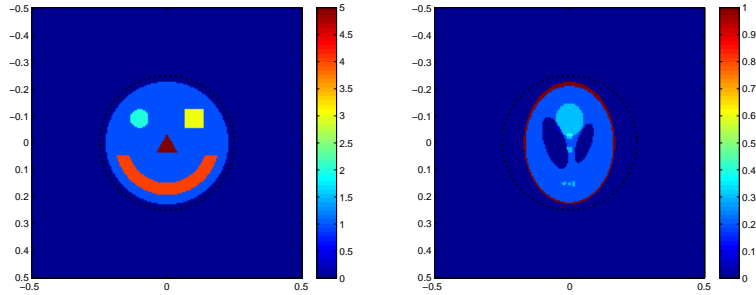


Figure 4.1: The phantoms Smiley and Shepp Logan.

Table 4.1: For each iteration  $l$  we show the residual  $\|\mathbf{r}^l\|_2$  of (3.2), the objective function value  $\mathcal{J}(\mathbf{f})$  of  $(P_0)$  and the number of the BICGSTAB iterations  $l_{\text{inner}}$ .

$l$	Smiley Face			Shepp Logan Phantom		
	$\ \mathbf{r}^l\ _2$	$\mathcal{J}(\mathbf{f}^l)$	$l_{\text{inner}}$	$\ \mathbf{r}^l\ _2$	$\mathcal{J}(\mathbf{f}^l)$	$l_{\text{inner}}$
0	0.0960	0.0923	-	0.0212	0.0084	-
1	0.0016	0.0081	30	9.66e-4	0.0028	24
2	7.53e-4	0.0068	21	4.79e-4	0.0024	19
3	7.04e-4	0.0066	16	1.50e-5	0.0024	43
4	4.88e-4	0.0065	13	1.68e-6	0.0023	44
5	1.07e-4	0.0065	16			
6	1.96e-7	0.0065	45			

Furthermore, for the comparison of computational efficiency, all simulations are run in MATLAB 7.11.0 (R2010b) on a laptop equipped with a P8700 2.53GHz CPU and 4GByte main memory.

*Example 1.* In this example, we give the reconstructed results from the spherical mean values of the phantoms shown in Figure 4.1 by solving the TV regularization model  $(P_0)$ . Here, the phantoms are assumed to be supported in the disk with the radius less than 0.25, and there are  $M_1 = 80$  detectors (shown as black dots in Figure 4.1) uniformly distributed on the surrounding circle. Since in this case the spherical mean values vanish for  $r > 0.5$ , the given data  $\mathbf{g}$  include the spherical mean values with  $0 \leq r \leq 0.5$ , which are discretized as  $M_2 = 100$  linearly equally spaced points. Hence, in this example we have  $M = 8000$ . In addition, the image resolution of the phantoms are 100-by-100, i.e.  $N = n^2 = 10^4$ . In Figure 4.2, we show the spherical mean values  $\mathbf{g}$  and the least squares solutions of (3.1) by solving  $\min_{\mathbf{f}} \frac{1}{2} \|\mathbf{M}\mathbf{f} - \mathbf{g}\|_2^2$ , which is utilized as the initial value in our primal-dual method for solving the TV-model.

When solving the minimization problem  $(P_0)$ , the regularization parameter is set to  $\alpha = 10^{-5}$ , and the stopping rule of the Newton iteration are reached after  $l = 6$  and  $l = 4$  iterations with the CPU time 222.1s and 173.3s, respectively. Figure 4.3 shows the reconstructed images in a few iterations. Comparing the final results with the original phantoms in Figure 4.1 and

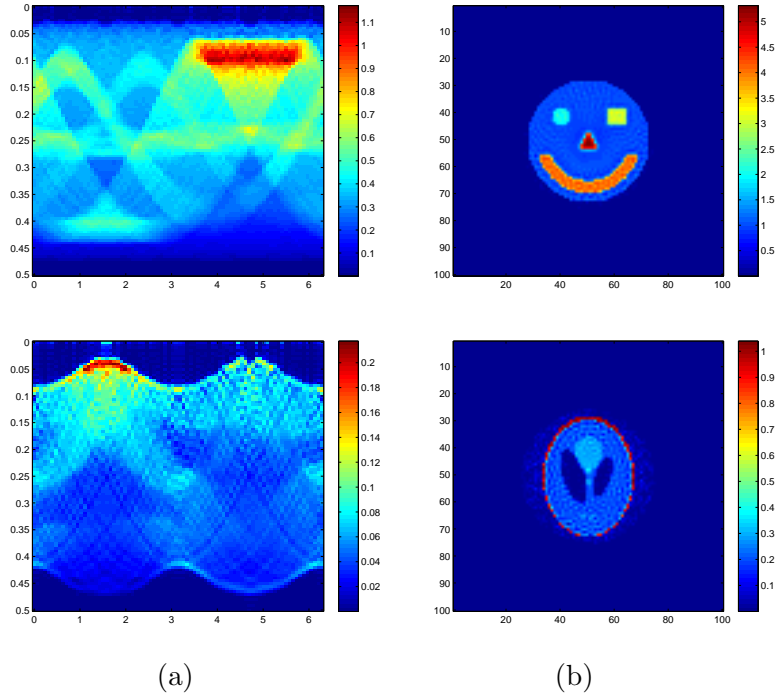


Figure 4.2: (a) The data  $\mathbf{g} \in \mathbb{R}^{M_1 \times M_2}$ , (b) the least squares solutions of (3.1), row 1: for the smiley face; row 2: for the Shepp Logan phantom.

the least squares solutions, we observe that the method based on the TV-model performs very good reconstructions. Furthermore, to illustrate the convergence behavior of our method for solving (3.2), in Table 4.1 we list the residuals of the system (3.2), the objective function values of  $(P_0)$ , and the number of the BICGSTAB algorithm in each Newton step. The decrease of the residual implies a locally superlinear convergence of the iterations.

*Example 2.* In order to show the computational efficiency, we compare our primal-dual method with an alternating minimization algorithm which utilizes the splitting technique to solve the TV-model  $(P_0)$ , see [18]. In the proposed algorithm, a quadratic penalty term is introduced in  $(P_0)$ , i.e.,

$$\min_{\mathbf{f} \in \mathbb{R}^N} \frac{1}{2} \|\mathbf{M}\mathbf{f} - \mathbf{g}\|_2^2 + \frac{\beta}{2} \|\mathbf{f} - \mathbf{u}\|_2^2 + \alpha \|\mathbf{u}\|_{\text{TV}}.$$

Then, the reconstructed image  $\mathbf{f}$  is obtained by solving the following two minimization problems

$$\begin{aligned} \mathbf{f}^l &= \operatorname{argmin}_{\mathbf{f} \in \mathbb{R}^N} \frac{1}{2} \|\mathbf{M}\mathbf{f} - \mathbf{g}\|_2^2 + \frac{\beta}{2} \|\mathbf{f} - \mathbf{u}^{l-1}\|_2^2, \\ \mathbf{u}^l &= \operatorname{argmin}_{\mathbf{u} \in \mathbb{R}^N} \frac{\beta}{2} \|\mathbf{f}^l - \mathbf{u}\|_2^2 + \alpha \|\mathbf{u}\|_{\text{TV}}, \end{aligned}$$

alternately. The objective function of the first optimization problem is quadratic, and it is solved by the conjugate gradient method. The second minimization problem is working on the image domain, and the Fenchel-duality-based Chambolle's method [6] is used to solve it

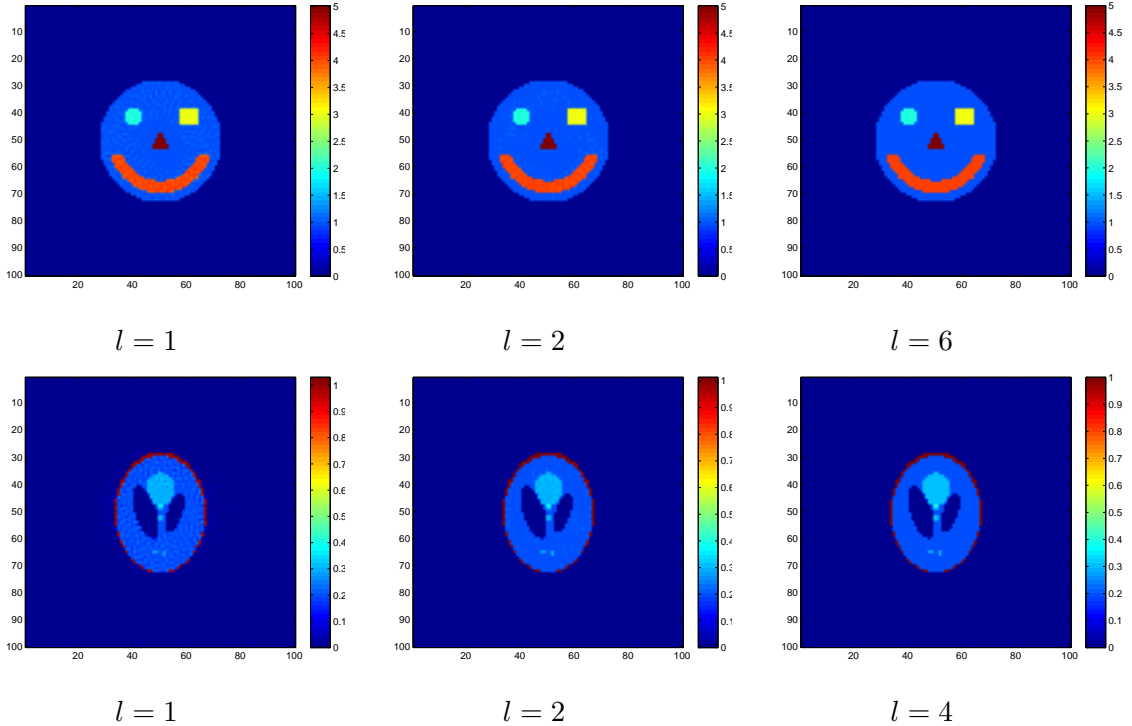


Figure 4.3: The reconstructed result in the Newton iteration during solving the TV-model.

as suggested in [18] with  $\beta = 3 \cdot 10^{-3}$ . Since both of the methods are solving approximations of  $(P_0)$ , to compare the computational efficiency, in Figure 4.4 we show the plots of the objective function values of  $(P_0)$  versus iterations with the same  $\alpha$ . In this example, we stop the splitting method after 200 iterations and it spends 6648.6 seconds. But the final function value is still larger than that from our method after 6 Newton iterations and 222.1s CPU time. It is easy to see that our method is much more efficient. In addition, we also give the reconstructed images obtained by both methods. Since the alternating algorithm and our primal-dual method both aim at minimizing the TV-model  $(P_0)$ , they obtain similar results. But comparing the intensity range of the results, our method performs more exact reconstruction, and the shrinkage in the result by the alternating minimization algorithm is due to the quadratic penalty function technique.

*Example 3.* Now, we test our algorithm for reconstructing the data corrupted by white Gaussian noise with different noise levels. In each case, we choose a reasonable parameter  $\alpha$  for it. In Figure 4.5, we give the data  $\mathbf{g}$  corrupted by 5% and 10% white Gaussian noise, respectively, and the corresponding reconstructed images by solving  $\min_{\mathbf{f}} \|\mathbf{M}\mathbf{f} - \mathbf{g}\|_2^2$ . The results obtained by our algorithm from solving the TV-model  $(P_0)$  are shown in Figure 4.6. Since the parameter  $\alpha$  controls the trade-off between a good fit of  $\mathbf{g}$  and a smoothness requirement due to the total variation regularization, to show the influence of the parameter  $\alpha$  on the reconstructions, we list two results with different values of  $\alpha$  for each noise level in Figure 4.6. It is seen that with larger  $\alpha$ , the reconstructed images are smoother, and the intensity range of the images are reduced obviously, which can be seen from the color bar on the right side of the images. However, with smaller  $\alpha$  the results include more details, but at

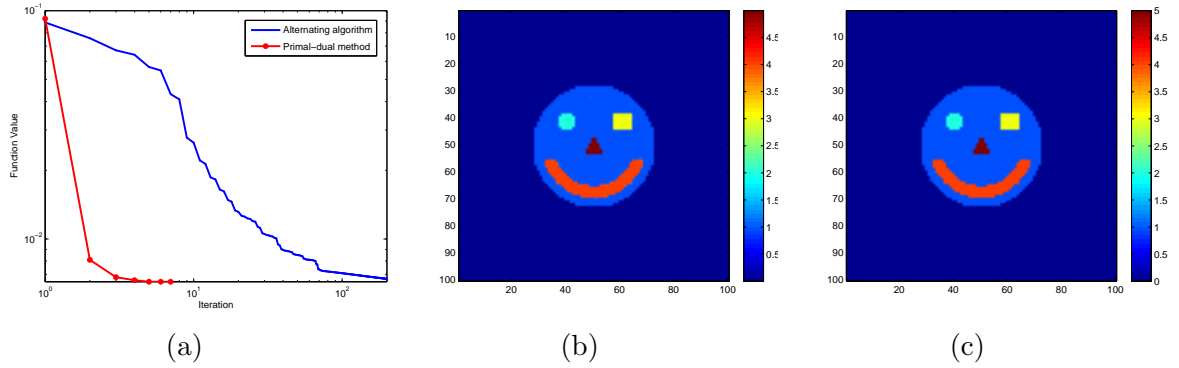


Figure 4.4: (a) The objective function values of  $(P_0)$  versus iterations, (b) the result from the alternating minimization algorithm proposed in [18], (c) the result from our primal-dual method.

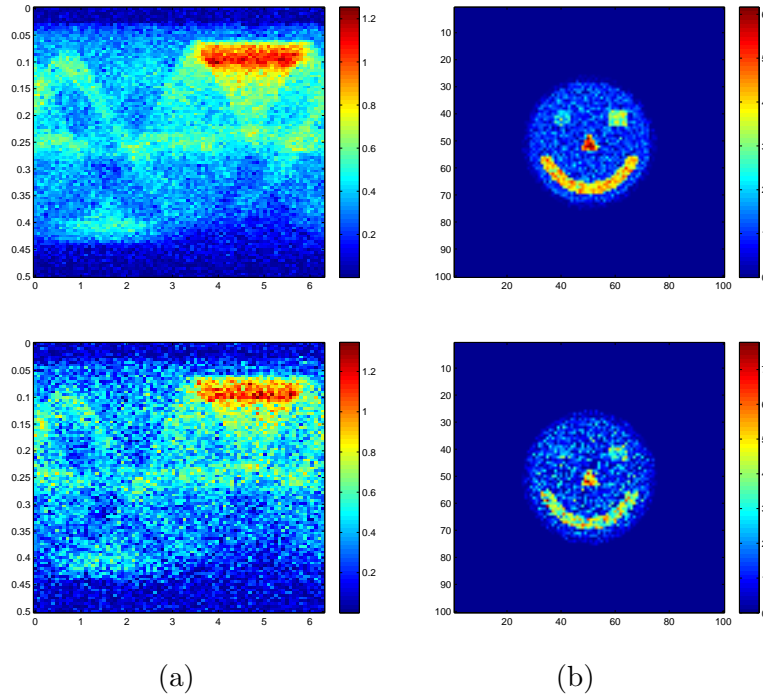


Figure 4.5: (a) With the noise level 5%; (b) with the noise level 10%. Row 1: the data  $\mathbf{g}$  with white Gaussian noise; row 2: the least squares solutions of (3.1).

the same time some noise is left.

In addition, in Table 4.2 we list the number of the Newton iterations, the total number of the BICGSTAB iterations and the CPU time. Here, the least squares solutions cannot supply good estimate as the initial vector  $\mathbf{f}^0$ , see Figure 4.5. Although in all our tests the numbers of Newton steps reach the maximum of 10 iterations, the reconstructed results are already acceptable. Based on our numerical experiments, allowing more iterations yields no

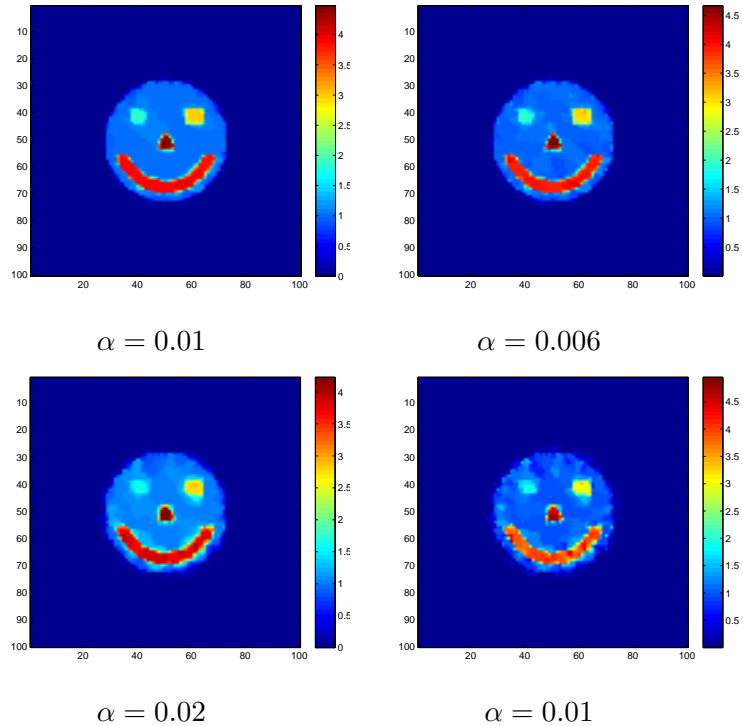


Figure 4.6: The reconstructed results by solving the TV-model with different parameter values and noise levels. Row 1: for noise level 5%; row 2: for noise level 10%.

Table 4.2: For different noise levels and  $\alpha$ , the number of Newton iterations  $l^{\text{all}}$ , the total number of the BICGSTAB iterations  $l_{\text{inner}}^{\text{all}}$ , and the CPU time  $t$ .

noise	5%		10%	
	0.01	0.006	0.02	0.01
$l^{\text{all}}$	10	10	10	10
$l_{\text{inner}}^{\text{all}}$	124	120	124	168
$t$	179.6	170.4	189.8	242.9

significant effect on the results.

*Example 4.* Since in many practical cases the detectors are only able to be located on a limited region in this example we consider that the detectors are uniformly distributed on the upper half circle instead of whole circle. In Figure 4.7, we give the data  $\mathbf{g}$ , and the least squares solution of (3.1), which is set as the initial guess of  $\mathbf{f}$  when solving the TV-model. In addition, Figure 4.7 also shows the reconstructed image with  $\alpha = 10^{-4}$  by our algorithm based on the TV-model and the plot of the residuals of the primal-dual system equations (3.2). We note that in this limited view case solving the TV-model by our primal-dual method still gives a good reconstruction.

*Example 5.* In this example, we consider the image size of phantoms as 200-by-200, i.e.

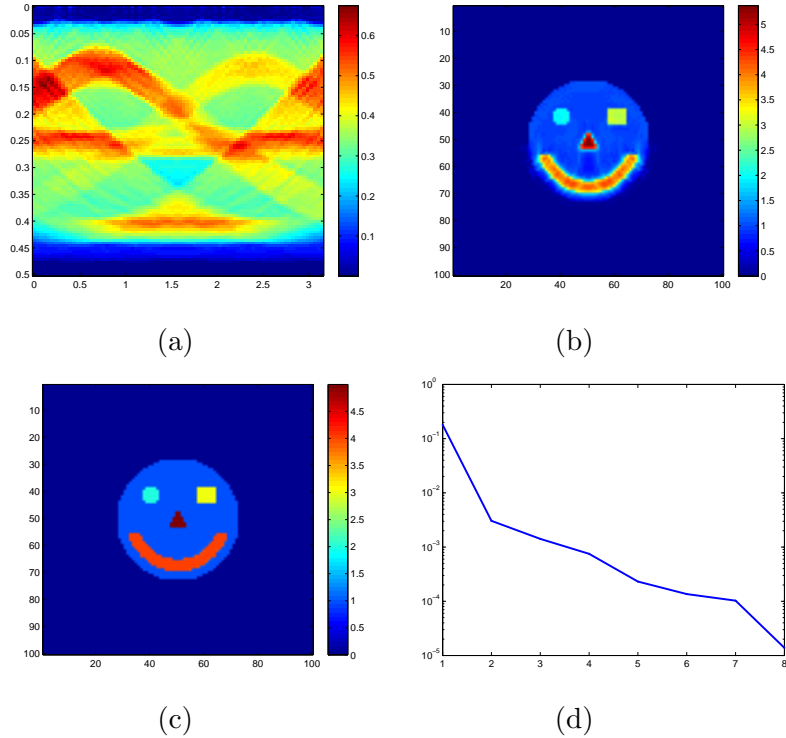


Figure 4.7: (a) The data  $\mathbf{g}$ , (b) the reconstructed result by solving  $\min \|\mathbf{M}\mathbf{f} - \mathbf{g}\|_2^2$ , (c) the result by solving  $(P_0)$ , (d) the residuals of the system equations (3.2) versus iterations.

$n = 200$ , and there are still  $M_1 = 80$  detectors uniformly distributed on the unit circle. But the range of the parameter  $r$  in the spherical mean values is discretized as  $M_2 = 200$  linearly equally spaced points. In Figure 4.8, we give the data  $\mathbf{g}$ , the least squares results, and the reconstructed images with  $\alpha = 6 \cdot 10^{-5}$  by solving the TV-model. By our method, the stopping rule is reached after  $l = 5$  and  $l = 10$  Newton iterations with the CPU time 2337.9s and 2431.5s, respectively.

## 5 Summary

We introduced a novel iterative reconstruction method in photoacoustic imaging which does not rely on a specific geometry of the detectors. Based on a dedicated discretization of the spherical mean value operator and a total variation regularizer, our method performs reasonable efficiently and preserves important features like edges in the reconstruction.

## Acknowledgment

The authors gratefully acknowledge support by the German Research Foundation within the project KU 2557/1-1 and by the Helmholtz Association within the young investigator group VH-NG-526.

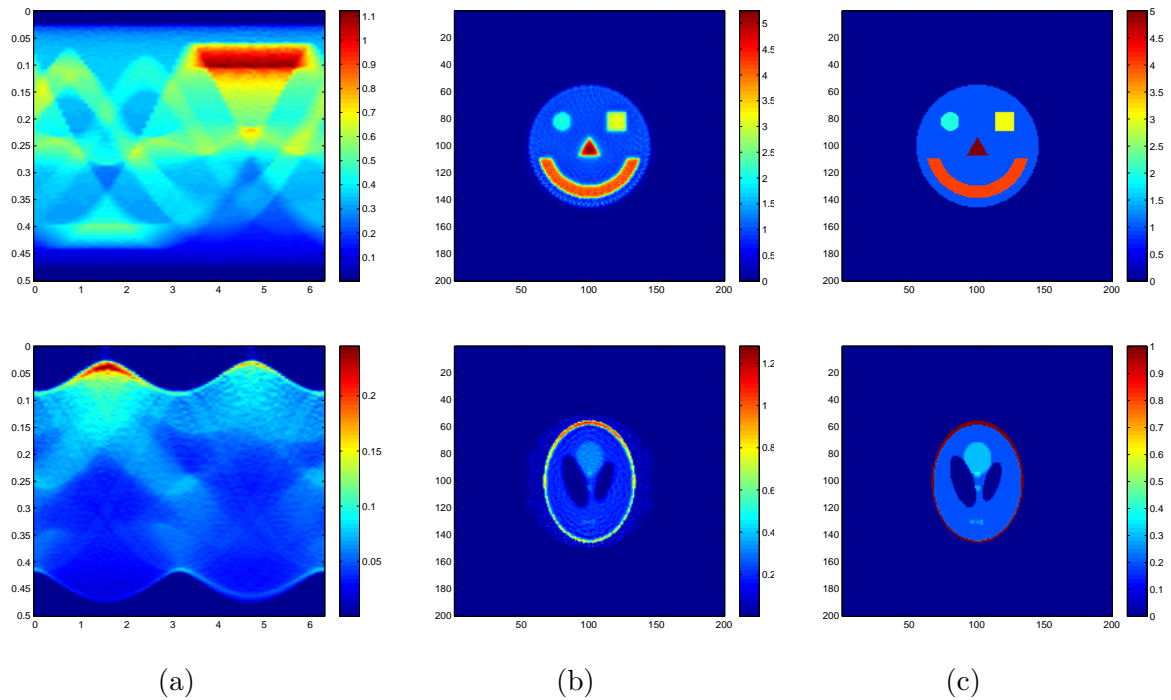


Figure 4.8: (a) The data  $g$ , (b) the least squares results, (c) the reconstructed result by solving  $(P_0)$ .

## References

- [1] M. Agranovsky and P. Kuchment. Uniqueness of reconstruction and an inversion procedure for thermoacoustic and photoacoustic tomography with variable sound speed. *Inverse Problems*, 23(5):2089–2102, 2007.
- [2] M. Agranovsky, P. Kuchment, and L. Kunyansky. On reconstruction formulas and algorithms for the thermoacoustic tomography. In L. V. Wang, editor, *Photoacoustic imaging and spectroscopy*, chapter 8, pages 89–101. CRC Press, Boca Raton, FL, 2009.
- [3] M. Agranovsky, P. Kuchment, and E. T. Quinto. Range descriptions for the spherical mean Radon transform. *J. Funct. Anal.*, 248(2):344–386, 2007.
- [4] A. Buehler, A. Rosenthal, T. Jetzfellner, A. Dima, D. Razansky, and V. Ntziachristos. Model-based optoacoustic inversions with incomplete projection data. *Med. Phys.*, 38(1694), 2011.
- [5] P. Burgholzer, G. J. Matt, M. Haltmeier, and G. Paltauf. Exact and approximate imaging methods for photoacoustic tomography using an arbitrary detection surface. *Phys. Rev. E*, 75(4):046706, 2007.
- [6] A. Chambolle. An algorithm for total variation minimization and applications. *J. Math. Imaging Vision*, 20(1-2):89–97, 2004. Special issue on mathematics and image analysis.
- [7] R. Courant and D. Hilbert. *Methods of mathematical physics. Vol. II: Partial differential*

- equations*. (Vol. II by R. Courant.). Interscience Publishers (a division of John Wiley & Sons), New York-London, 1962.
- [8] F. Filbir, R. Hielscher, and W. R. Madych. Reconstruction from circular and spherical mean data. *Appl. Comput. Harmon. Anal.*, 29(1):111–120, 2010.
  - [9] D. Finch, M. Haltmeier, and Rakesh. Inversion of spherical means and the wave equation in even dimensions. *SIAM J. Appl. Math.*, 68(2):392–412, 2007.
  - [10] T. Görner, R. Hielscher, and S. Kunis. Efficient and accurate computation of spherical mean values at scattered center points. *Preprint*, 2011.
  - [11] M. Haltmeier. A mollification approach for inverting the spherical mean radon transform. *SIAM J. Appl. Math.*, 71(5):1637–1652, 2011.
  - [12] M. Haltmeier, O. Scherzer, P. Burgholzer, and G. Paltauf. Thermoacoustic computed tomography with large planar receivers. *Inverse Problems*, 20(5):1663–1673, 2004.
  - [13] M. Haltmeier, O. Scherzer, and G. Zangerl. A reconstruction algorithm for photoacoustic imaging based on the nonuniform FFT. *IEEE Trans. Med. Imag.*, 28(11):1727–1735, 2009.
  - [14] M. Haltmeier, T. Schuster, and O. Scherzer. Filtered backprojection for thermoacoustic computed tomography in spherical geometry. *Math. Methods Appl. Sci.*, 28(16):1919–1937, 2005.
  - [15] M. Haltmeier and G. Zangerl. Spatial resolution in photoacoustic tomography: effects of detector size and detector bandwidth. *Inverse Problems*, 26(12):125002, 14, 2010.
  - [16] M. Hintermüller, K. Ito, and K. Kunisch. The primal-dual active set strategy as a semismooth Newton method. *SIAM J. Optim.*, 13(3):865–888 (2003), 2002.
  - [17] M. Hintermüller and G. Stadler. An infeasible primal-dual algorithm for total bounded variation-based inf-convolution-type image restoration. *SIAM J. Sci. Comput.*, 28(1):1–23, 2006.
  - [18] Y. Huang, M. K. Ng, and Y.-W. Wen. A fast total variation minimization method for image restoration. *Multiscale Model. Simul.*, 7(2):774–795, 2008.
  - [19] P. J. Huber. Robust regression: asymptotics, conjectures and Monte Carlo. *Ann. Statist.*, 1:799–821, 1973.
  - [20] J. Keiner, S. Kunis, and D. Potts. Using NFFT 3—a software library for various nonequispaced fast Fourier transforms. *ACM Trans. Math. Software*, 36(4):Art. 19, 30, 2009.
  - [21] P. Kuchment and L. Kunyansky. Mathematics of thermoacoustic tomography. *European J. Appl. Math.*, 19(2):191–224, 2008.
  - [22] S. Kunis and I. Melzer. On the butterfly sparse Fourier transform. *Preprint*, 2011.
  - [23] L. Kunyansky. Reconstruction of a function from its spherical (circular) means with the centers lying on the surface of certain polygons and polyhedra. *Inverse Problems*, 27(2):025012, 22, 2011.

- [24] L. A. Kunyansky. Explicit inversion formulae for the spherical mean Radon transform. *Inverse Problems*, 23(1):373–383, 2007.
- [25] L. A. Kunyansky. A series solution and a fast algorithm for the inversion of the spherical mean Radon transform. *Inverse Problems*, 23(6):S11–S20, 2007.
- [26] G. Paltauf, R. Nuster, M. Haltmeier, and P. Burgholzer. Photoacoustic tomography with integrating area and line detectors. In L. V. Wang, editor, *Photoacoustic Imaging and Spectroscopy*, Optical Science and Engineering, chapter 20, pages 251–263. CRC Press, Boca Raton, FL, 2009.
- [27] L. Q. Qi and J. Sun. A nonsmooth version of Newton’s method. *Math. Programming*, 58(3, Ser. A):353–367, 1993.
- [28] E. T. Quinto. Helgason’s support theorem and spherical Radon transforms. In *Radon transforms, geometry, and wavelets*, volume 464 of *Contemp. Math.*, pages 249–264. Amer. Math. Soc., Providence, RI, 2008.
- [29] L. Rudin, S. Osher, and E. Fatemi. Nonlinear total variation based noise removal algorithms. *Physica D*, 60:259–268, 1992.
- [30] Y. Saad. *Iterative methods for sparse linear systems*. Society for Industrial and Applied Mathematics, Philadelphia, PA, second edition, 2003.
- [31] L. V. Wang and H. Wu. *Biomedical Optics - Principles and Imaging*. John Wiley & Sons Inc., Hoboken, NJ, 2007.
- [32] L. Ying. Sparse Fourier transform via butterfly algorithm. *SIAM J. Sci. Comput.*, 31(3):1678–1694, 2009.
- [33] G. Zangerl and O. Scherzer. Exact reconstruction in photoacoustic tomography with circular integrating detectors II: spherical geometry. *Math. Methods Appl. Sci.*, 33(15):1771–1782, 2010.
- [34] G. Zangerl, O. Scherzer, and M. Haltmeier. Exact series reconstruction in photoacoustic tomography with circular integrating detectors. *Commun. Math. Sci.*, 7(3):665–678, 2009.

# Preprint Series DFG-SPP 1324

<http://www.dfg-spp1324.de>

## Reports

- [1] R. Ramlau, G. Teschke, and M. Zhariy. A Compressive Landweber Iteration for Solving Ill-Posed Inverse Problems. Preprint 1, DFG-SPP 1324, September 2008.
- [2] G. Plonka. The Easy Path Wavelet Transform: A New Adaptive Wavelet Transform for Sparse Representation of Two-dimensional Data. Preprint 2, DFG-SPP 1324, September 2008.
- [3] E. Novak and H. Woźniakowski. Optimal Order of Convergence and (In-) Tractability of Multivariate Approximation of Smooth Functions. Preprint 3, DFG-SPP 1324, October 2008.
- [4] M. Espig, L. Grasedyck, and W. Hackbusch. Black Box Low Tensor Rank Approximation Using Fibre-Crosses. Preprint 4, DFG-SPP 1324, October 2008.
- [5] T. Bonesky, S. Dahlke, P. Maass, and T. Raasch. Adaptive Wavelet Methods and Sparsity Reconstruction for Inverse Heat Conduction Problems. Preprint 5, DFG-SPP 1324, January 2009.
- [6] E. Novak and H. Woźniakowski. Approximation of Infinitely Differentiable Multivariate Functions Is Intractable. Preprint 6, DFG-SPP 1324, January 2009.
- [7] J. Ma and G. Plonka. A Review of Curvelets and Recent Applications. Preprint 7, DFG-SPP 1324, February 2009.
- [8] L. Denis, D. A. Lorenz, and D. Tiede. Greedy Solution of Ill-Posed Problems: Error Bounds and Exact Inversion. Preprint 8, DFG-SPP 1324, April 2009.
- [9] U. Friedrich. A Two Parameter Generalization of Lions' Nonoverlapping Domain Decomposition Method for Linear Elliptic PDEs. Preprint 9, DFG-SPP 1324, April 2009.
- [10] K. Bredies and D. A. Lorenz. Minimization of Non-smooth, Non-convex Functionals by Iterative Thresholding. Preprint 10, DFG-SPP 1324, April 2009.
- [11] K. Bredies and D. A. Lorenz. Regularization with Non-convex Separable Constraints. Preprint 11, DFG-SPP 1324, April 2009.

- [12] M. Döhler, S. Kunis, and D. Potts. Nonequispaced Hyperbolic Cross Fast Fourier Transform. Preprint 12, DFG-SPP 1324, April 2009.
- [13] C. Bender. Dual Pricing of Multi-Exercise Options under Volume Constraints. Preprint 13, DFG-SPP 1324, April 2009.
- [14] T. Müller-Gronbach and K. Ritter. Variable Subspace Sampling and Multi-level Algorithms. Preprint 14, DFG-SPP 1324, May 2009.
- [15] G. Plonka, S. Tenorth, and A. Iske. Optimally Sparse Image Representation by the Easy Path Wavelet Transform. Preprint 15, DFG-SPP 1324, May 2009.
- [16] S. Dahlke, E. Novak, and W. Sickel. Optimal Approximation of Elliptic Problems by Linear and Nonlinear Mappings IV: Errors in  $L_2$  and Other Norms. Preprint 16, DFG-SPP 1324, June 2009.
- [17] B. Jin, T. Khan, P. Maass, and M. Pidcock. Function Spaces and Optimal Currents in Impedance Tomography. Preprint 17, DFG-SPP 1324, June 2009.
- [18] G. Plonka and J. Ma. Curvelet-Wavelet Regularized Split Bregman Iteration for Compressed Sensing. Preprint 18, DFG-SPP 1324, June 2009.
- [19] G. Teschke and C. Borries. Accelerated Projected Steepest Descent Method for Nonlinear Inverse Problems with Sparsity Constraints. Preprint 19, DFG-SPP 1324, July 2009.
- [20] L. Grasedyck. Hierarchical Singular Value Decomposition of Tensors. Preprint 20, DFG-SPP 1324, July 2009.
- [21] D. Rudolf. Error Bounds for Computing the Expectation by Markov Chain Monte Carlo. Preprint 21, DFG-SPP 1324, July 2009.
- [22] M. Hansen and W. Sickel. Best  $m$ -term Approximation and Lizorkin-Triebel Spaces. Preprint 22, DFG-SPP 1324, August 2009.
- [23] F.J. Hickernell, T. Müller-Gronbach, B. Niu, and K. Ritter. Multi-level Monte Carlo Algorithms for Infinite-dimensional Integration on  $\mathbb{R}^N$ . Preprint 23, DFG-SPP 1324, August 2009.
- [24] S. Dereich and F. Heidenreich. A Multilevel Monte Carlo Algorithm for Lévy Driven Stochastic Differential Equations. Preprint 24, DFG-SPP 1324, August 2009.
- [25] S. Dahlke, M. Fornasier, and T. Raasch. Multilevel Preconditioning for Adaptive Sparse Optimization. Preprint 25, DFG-SPP 1324, August 2009.

- [26] S. Dereich. Multilevel Monte Carlo Algorithms for Lévy-driven SDEs with Gaussian Correction. Preprint 26, DFG-SPP 1324, August 2009.
- [27] G. Plonka, S. Tenorth, and D. Roşca. A New Hybrid Method for Image Approximation using the Easy Path Wavelet Transform. Preprint 27, DFG-SPP 1324, October 2009.
- [28] O. Koch and C. Lubich. Dynamical Low-rank Approximation of Tensors. Preprint 28, DFG-SPP 1324, November 2009.
- [29] E. Faou, V. Gradinaru, and C. Lubich. Computing Semi-classical Quantum Dynamics with Hagedorn Wavepackets. Preprint 29, DFG-SPP 1324, November 2009.
- [30] D. Conte and C. Lubich. An Error Analysis of the Multi-configuration Time-dependent Hartree Method of Quantum Dynamics. Preprint 30, DFG-SPP 1324, November 2009.
- [31] C. E. Powell and E. Ullmann. Preconditioning Stochastic Galerkin Saddle Point Problems. Preprint 31, DFG-SPP 1324, November 2009.
- [32] O. G. Ernst and E. Ullmann. Stochastic Galerkin Matrices. Preprint 32, DFG-SPP 1324, November 2009.
- [33] F. Lindner and R. L. Schilling. Weak Order for the Discretization of the Stochastic Heat Equation Driven by Impulsive Noise. Preprint 33, DFG-SPP 1324, November 2009.
- [34] L. Kämmerer and S. Kunis. On the Stability of the Hyperbolic Cross Discrete Fourier Transform. Preprint 34, DFG-SPP 1324, December 2009.
- [35] P. Cerejeiras, M. Ferreira, U. Kähler, and G. Teschke. Inversion of the noisy Radon transform on  $SO(3)$  by Gabor frames and sparse recovery principles. Preprint 35, DFG-SPP 1324, January 2010.
- [36] T. Jahnke and T. Udrescu. Solving Chemical Master Equations by Adaptive Wavelet Compression. Preprint 36, DFG-SPP 1324, January 2010.
- [37] P. Kittipoom, G. Kutyniok, and W.-Q. Lim. Irregular Shearlet Frames: Geometry and Approximation Properties. Preprint 37, DFG-SPP 1324, February 2010.
- [38] G. Kutyniok and W.-Q. Lim. Compactly Supported Shearlets are Optimally Sparse. Preprint 38, DFG-SPP 1324, February 2010.

- [39] M. Hansen and W. Sickel. Best  $m$ -Term Approximation and Tensor Products of Sobolev and Besov Spaces – the Case of Non-compact Embeddings. Preprint 39, DFG-SPP 1324, March 2010.
- [40] B. Niu, F.J. Hickernell, T. Müller-Gronbach, and K. Ritter. Deterministic Multi-level Algorithms for Infinite-dimensional Integration on  $\mathbb{R}^N$ . Preprint 40, DFG-SPP 1324, March 2010.
- [41] P. Kittipoom, G. Kutyniok, and W.-Q Lim. Construction of Compactly Supported Shearlet Frames. Preprint 41, DFG-SPP 1324, March 2010.
- [42] C. Bender and J. Steiner. Error Criteria for Numerical Solutions of Backward SDEs. Preprint 42, DFG-SPP 1324, April 2010.
- [43] L. Grasedyck. Polynomial Approximation in Hierarchical Tucker Format by Vector-Tensorization. Preprint 43, DFG-SPP 1324, April 2010.
- [44] M. Hansen und W. Sickel. Best  $m$ -Term Approximation and Sobolev-Besov Spaces of Dominating Mixed Smoothness - the Case of Compact Embeddings. Preprint 44, DFG-SPP 1324, April 2010.
- [45] P. Binev, W. Dahmen, and P. Lamby. Fast High-Dimensional Approximation with Sparse Occupancy Trees. Preprint 45, DFG-SPP 1324, May 2010.
- [46] J. Ballani and L. Grasedyck. A Projection Method to Solve Linear Systems in Tensor Format. Preprint 46, DFG-SPP 1324, May 2010.
- [47] P. Binev, A. Cohen, W. Dahmen, R. DeVore, G. Petrova, and P. Wojtaszczyk. Convergence Rates for Greedy Algorithms in Reduced Basis Methods. Preprint 47, DFG-SPP 1324, May 2010.
- [48] S. Kestler and K. Urban. Adaptive Wavelet Methods on Unbounded Domains. Preprint 48, DFG-SPP 1324, June 2010.
- [49] H. Yserentant. The Mixed Regularity of Electronic Wave Functions Multiplied by Explicit Correlation Factors. Preprint 49, DFG-SPP 1324, June 2010.
- [50] H. Yserentant. On the Complexity of the Electronic Schrödinger Equation. Preprint 50, DFG-SPP 1324, June 2010.
- [51] M. Guillemard and A. Iske. Curvature Analysis of Frequency Modulated Manifolds in Dimensionality Reduction. Preprint 51, DFG-SPP 1324, June 2010.
- [52] E. Herrholz and G. Teschke. Compressive Sensing Principles and Iterative Sparse Recovery for Inverse and Ill-Posed Problems. Preprint 52, DFG-SPP 1324, July 2010.

- [53] L. Kämmerer, S. Kunis, and D. Potts. Interpolation Lattices for Hyperbolic Cross Trigonometric Polynomials. Preprint 53, DFG-SPP 1324, July 2010.
- [54] G. Kutyniok and W.-Q Lim. Shearlets on Bounded Domains. Preprint 54, DFG-SPP 1324, July 2010.
- [55] A. Zeiser. Wavelet Approximation in Weighted Sobolev Spaces of Mixed Order with Applications to the Electronic Schrödinger Equation. Preprint 55, DFG-SPP 1324, July 2010.
- [56] G. Kutyniok, J. Lemvig, and W.-Q Lim. Compactly Supported Shearlets. Preprint 56, DFG-SPP 1324, July 2010.
- [57] A. Zeiser. On the Optimality of the Inexact Inverse Iteration Coupled with Adaptive Finite Element Methods. Preprint 57, DFG-SPP 1324, July 2010.
- [58] S. Jokar. Sparse Recovery and Kronecker Products. Preprint 58, DFG-SPP 1324, August 2010.
- [59] T. Aboiyar, E. H. Georgoulis, and A. Iske. Adaptive ADER Methods Using Kernel-Based Polyharmonic Spline WENO Reconstruction. Preprint 59, DFG-SPP 1324, August 2010.
- [60] O. G. Ernst, A. Mugler, H.-J. Starkloff, and E. Ullmann. On the Convergence of Generalized Polynomial Chaos Expansions. Preprint 60, DFG-SPP 1324, August 2010.
- [61] S. Holtz, T. Rohwedder, and R. Schneider. On Manifolds of Tensors of Fixed TT-Rank. Preprint 61, DFG-SPP 1324, September 2010.
- [62] J. Ballani, L. Grasedyck, and M. Kluge. Black Box Approximation of Tensors in Hierarchical Tucker Format. Preprint 62, DFG-SPP 1324, October 2010.
- [63] M. Hansen. On Tensor Products of Quasi-Banach Spaces. Preprint 63, DFG-SPP 1324, October 2010.
- [64] S. Dahlke, G. Steidl, and G. Teschke. Shearlet Coorbit Spaces: Compactly Supported Analyzing Shearlets, Traces and Embeddings. Preprint 64, DFG-SPP 1324, October 2010.
- [65] W. Hackbusch. Tensorisation of Vectors and their Efficient Convolution. Preprint 65, DFG-SPP 1324, November 2010.
- [66] P. A. Cioica, S. Dahlke, S. Kinzel, F. Lindner, T. Raasch, K. Ritter, and R. L. Schilling. Spatial Besov Regularity for Stochastic Partial Differential Equations on Lipschitz Domains. Preprint 66, DFG-SPP 1324, November 2010.

- [67] E. Novak and H. Woźniakowski. On the Power of Function Values for the Approximation Problem in Various Settings. Preprint 67, DFG-SPP 1324, November 2010.
- [68] A. Hinrichs, E. Novak, and H. Woźniakowski. The Curse of Dimensionality for Monotone and Convex Functions of Many Variables. Preprint 68, DFG-SPP 1324, November 2010.
- [69] G. Kutyniok and W.-Q. Lim. Image Separation Using Shearlets. Preprint 69, DFG-SPP 1324, November 2010.
- [70] B. Jin and P. Maass. An Analysis of Electrical Impedance Tomography with Applications to Tikhonov Regularization. Preprint 70, DFG-SPP 1324, December 2010.
- [71] S. Holtz, T. Rohwedder, and R. Schneider. The Alternating Linear Scheme for Tensor Optimisation in the TT Format. Preprint 71, DFG-SPP 1324, December 2010.
- [72] T. Müller-Gronbach and K. Ritter. A Local Refinement Strategy for Constructive Quantization of Scalar SDEs. Preprint 72, DFG-SPP 1324, December 2010.
- [73] T. Rohwedder and R. Schneider. An Analysis for the DIIS Acceleration Method used in Quantum Chemistry Calculations. Preprint 73, DFG-SPP 1324, December 2010.
- [74] C. Bender and J. Steiner. Least-Squares Monte Carlo for Backward SDEs. Preprint 74, DFG-SPP 1324, December 2010.
- [75] C. Bender. Primal and Dual Pricing of Multiple Exercise Options in Continuous Time. Preprint 75, DFG-SPP 1324, December 2010.
- [76] H. Harbrecht, M. Peters, and R. Schneider. On the Low-rank Approximation by the Pivoted Cholesky Decomposition. Preprint 76, DFG-SPP 1324, December 2010.
- [77] P. A. Cioica, S. Dahlke, N. Döhring, S. Kinzel, F. Lindner, T. Raasch, K. Ritter, and R. L. Schilling. Adaptive Wavelet Methods for Elliptic Stochastic Partial Differential Equations. Preprint 77, DFG-SPP 1324, January 2011.
- [78] G. Plonka, S. Tenorth, and A. Iske. Optimal Representation of Piecewise Hölder Smooth Bivariate Functions by the Easy Path Wavelet Transform. Preprint 78, DFG-SPP 1324, January 2011.

- [79] A. Mugler and H.-J. Starkloff. On Elliptic Partial Differential Equations with Random Coefficients. Preprint 79, DFG-SPP 1324, January 2011.
- [80] T. Müller-Gronbach, K. Ritter, and L. Yaroslavtseva. A Derandomization of the Euler Scheme for Scalar Stochastic Differential Equations. Preprint 80, DFG-SPP 1324, January 2011.
- [81] W. Dahmen, C. Huang, C. Schwab, and G. Welper. Adaptive Petrov-Galerkin methods for first order transport equations. Preprint 81, DFG-SPP 1324, January 2011.
- [82] K. Grella and C. Schwab. Sparse Tensor Spherical Harmonics Approximation in Radiative Transfer. Preprint 82, DFG-SPP 1324, January 2011.
- [83] D.A. Lorenz, S. Schiffler, and D. Trede. Beyond Convergence Rates: Exact Inversion With Tikhonov Regularization With Sparsity Constraints. Preprint 83, DFG-SPP 1324, January 2011.
- [84] S. Dereich, M. Scheutzow, and R. Schottstedt. Constructive quantization: Approximation by empirical measures. Preprint 84, DFG-SPP 1324, January 2011.
- [85] S. Dahlke and W. Sickel. On Besov Regularity of Solutions to Nonlinear Elliptic Partial Differential Equations. Preprint 85, DFG-SPP 1324, January 2011.
- [86] S. Dahlke, U. Friedrich, P. Maass, T. Raasch, and R.A. Ressel. An adaptive wavelet method for parameter identification problems in parabolic partial differential equations. Preprint 86, DFG-SPP 1324, January 2011.
- [87] A. Cohen, W. Dahmen, and G. Welper. Adaptivity and Variational Stabilization for Convection-Diffusion Equations. Preprint 87, DFG-SPP 1324, January 2011.
- [88] T. Jahnke. On Reduced Models for the Chemical Master Equation. Preprint 88, DFG-SPP 1324, January 2011.
- [89] P. Binev, W. Dahmen, R. DeVore, P. Lamby, D. Savu, and R. Sharpley. Compressed Sensing and Electron Microscopy. Preprint 89, DFG-SPP 1324, March 2011.
- [90] P. Binev, F. Blanco-Silva, D. Blom, W. Dahmen, P. Lamby, R. Sharpley, and T. Vogt. High Quality Image Formation by Nonlocal Means Applied to High-Angle Annular Dark Field Scanning Transmission Electron Microscopy (HAADF-STEM). Preprint 90, DFG-SPP 1324, March 2011.
- [91] R. A. Ressel. A Parameter Identification Problem for a Nonlinear Parabolic Differential Equation. Preprint 91, DFG-SPP 1324, May 2011.

- [92] G. Kutyniok. Data Separation by Sparse Representations. Preprint 92, DFG-SPP 1324, May 2011.
- [93] M. A. Davenport, M. F. Duarte, Y. C. Eldar, and G. Kutyniok. Introduction to Compressed Sensing. Preprint 93, DFG-SPP 1324, May 2011.
- [94] H.-C. Kreuzler and H. Yserentant. The Mixed Regularity of Electronic Wave Functions in Fractional Order and Weighted Sobolev Spaces. Preprint 94, DFG-SPP 1324, June 2011.
- [95] E. Ullmann, H. C. Elman, and O. G. Ernst. Efficient Iterative Solvers for Stochastic Galerkin Discretizations of Log-Transformed Random Diffusion Problems. Preprint 95, DFG-SPP 1324, June 2011.
- [96] S. Kunis and I. Melzer. On the Butterfly Sparse Fourier Transform. Preprint 96, DFG-SPP 1324, June 2011.
- [97] T. Rohwedder. The Continuous Coupled Cluster Formulation for the Electronic Schrödinger Equation. Preprint 97, DFG-SPP 1324, June 2011.
- [98] T. Rohwedder and R. Schneider. Error Estimates for the Coupled Cluster Method. Preprint 98, DFG-SPP 1324, June 2011.
- [99] P. A. Cioica and S. Dahlke. Spatial Besov Regularity for Semilinear Stochastic Partial Differential Equations on Bounded Lipschitz Domains. Preprint 99, DFG-SPP 1324, July 2011.
- [100] L. Grasedyck and W. Hackbusch. An Introduction to Hierarchical (H-) Rank and TT-Rank of Tensors with Examples. Preprint 100, DFG-SPP 1324, August 2011.
- [101] N. Chegini, S. Dahlke, U. Friedrich, and R. Stevenson. Piecewise Tensor Product Wavelet Bases by Extensions and Approximation Rates. Preprint 101, DFG-SPP 1324, September 2011.
- [102] S. Dahlke, P. Oswald, and T. Raasch. A Note on Quarkonial Systems and Multi-level Partition of Unity Methods. Preprint 102, DFG-SPP 1324, September 2011.
- [103] A. Uschmajew. Local Convergence of the Alternating Least Squares Algorithm For Canonical Tensor Approximation. Preprint 103, DFG-SPP 1324, September 2011.
- [104] S. Kvaal. Multiconfigurational time-dependent Hartree method for describing particle loss due to absorbing boundary conditions. Preprint 104, DFG-SPP 1324, September 2011.

- [105] M. Guillemard and A. Iske. On Groupoid  $C^*$ -Algebras, Persistent Homology and Time-Frequency Analysis. Preprint 105, DFG-SPP 1324, September 2011.
- [106] A. Hinrichs, E. Novak, and H. Woźniakowski. Discontinuous information in the worst case and randomized settings. Preprint 106, DFG-SPP 1324, September 2011.
- [107] M. Espig, W. Hackbusch, A. Litvinenko, H. Matthies, and E. Zander. Efficient Analysis of High Dimensional Data in Tensor Formats. Preprint 107, DFG-SPP 1324, September 2011.
- [108] M. Espig, W. Hackbusch, S. Handschuh, and R. Schneider. Optimization Problems in Contracted Tensor Networks. Preprint 108, DFG-SPP 1324, October 2011.
- [109] S. Dereich, T. Müller-Gronbach, and K. Ritter. On the Complexity of Computing Quadrature Formulas for SDEs. Preprint 109, DFG-SPP 1324, October 2011.
- [110] D. Belomestny. Solving optimal stopping problems by empirical dual optimization and penalization. Preprint 110, DFG-SPP 1324, November 2011.
- [111] D. Belomestny and J. Schoenmakers. Multilevel dual approach for pricing American style derivatives. Preprint 111, DFG-SPP 1324, November 2011.
- [112] T. Rohwedder and A. Uschmajew. Local convergence of alternating schemes for optimization of convex problems in the TT format. Preprint 112, DFG-SPP 1324, December 2011.
- [113] T. Görner, R. Hielscher, and S. Kunis. Efficient and accurate computation of spherical mean values at scattered center points. Preprint 113, DFG-SPP 1324, December 2011.
- [114] Y. Dong, T. Görner, and S. Kunis. An iterative reconstruction scheme for photoacoustic imaging. Preprint 114, DFG-SPP 1324, December 2011.